JOURNAL OF MATERIALS SCIENCE 27 (1992) 5585–5590

Characterization of sputter-deposited 316L stainless steel films

M. J. GODBOLE, A. J. PEDRAZA
Materials Science and Engineering, University of Tennessee, Knoxville, TN 37996, USA
L. F. ALLARD
High Temperature Materials Laboratory, Oak Ridge National Laboratory, Oak Ridge, TN 37831, USA
G. GEESEY
College of Engineering, Montana State University, Bozeman, MT 59717, USA

Sputter-deposited 316L stainless steel films deposited on various substrates were characterized using transmission electron microscopy and X-ray diffractometry. The deposits were found to be fine-grained and the phases present in the films depended on the nature of the substrate. Films of various thicknesses deposited on microscope slides or oxidized stainless steel substrates contained a mixture of two phases: a body centre cubic (bcc) and a modified hexagonal ε-phase. The hexagonal phase appeared to be an ordered phase, as suggested by the a_0 value of the structure, which is twice that for the ε-martensite found in many deformed stainless steels. These films were hard and brittle, as indicated by microhardness measurements. Films deposited on oxide-free austenitic stainless steel substrates, on the other hand, were mostly bcc and exhibited a dominant ⟨200⟩ texture. These films were softer and less brittle than those deposited on oxidized substrates. *In situ* high-temperature X-ray diffractometry revealed that the ε-phase transformed to bcc when the films were annealed at 773 K. On annealing at 873 K, the bcc phase transformed to face centre cubic, which remained stable on cooling to room temperature. These results agree with published data which suggest stability of the bcc phase up to 840 K. Some discrepancies from earlier published reports are discussed in the light of the present results.

1. Introduction

Several investigations of sputter-deposited austenitic stainless steel films have demonstrated the predicted metastability of those steels at room temperature [1]. Malavasi *et al.* [2] studied the structure of AISI 304 and 316 stainless steel (304-SS and 316-SS) sputter-deposited on polished and ion-cleaned steel or plain glass substrates. The compositions of these two steels were somewhat similar, the major difference being the molybdenum content of the 316-SS. Both films exhibited a body centre cubic (bcc) structure when the target material itself was face centre cubic (fcc). However, sputter deposition of films from targets richer in chromium and/or nickel (Fe–20CR–25Ni, for instance) resulted in the formation of $\gamma + \alpha$ mixture of phases, and amorphous films were obtained when their carbon content was greater than 3 wt %.

Dahlgren [3] examined the structure of 304L-SS films sputter-deposited at temperatures in the range 274–1073 K on sputter-cleaned pre-polished 304-SS and oxygen-free high-conductivity (OFHC) copper substrates. The structure observed for depositions performed below 648 K was bcc, whereas a mixture of bcc and fcc structures formed between 648 and 773 K. Samples deposited at 773 and 1073 K were comprised primarily of fcc austenite accompanied by another unknown phase. Samples deposited at 274 K contained, in addition to bcc, an hcp-like phase which remained stable even after heating to 898 K. Wang [4] reported that a bcc structure formed in 304-SS films sputter-deposited at room temperature. By contrast, Grundy and Marsh [5] observed, in films deposited at room temperature, crystalline phases which could not be indexed as either an fcc or a bcc structure, and concluded that two phases were present in these films. On the other hand, sputter-deposition of 304-SS at 77 K yielded an amorphous structure [5]. Table I summarizes the experimental results just reviewed. Annealing above 823 K caused as-sputtered bcc phase in 304-SS to transform to fcc [6].

The microstructure of sputter-deposited films depends on the rate of deposition and substrate temperature. Factors such as working gas pressure and target–substrate distance influence the rate of deposition [7]. Lattice constants for the deposits made at 274 and 473 K were larger than those from deposits made at temperatures above 573 K [3]. No difference was seen in the lattice constant of fcc structure in the film and the parent material.

In the present work we have characterized both thick and thin films of 316L-SS sputter-deposited on various substrates. Thin films were characterized

0022–2461

TABLE I Summary of the reviewed experimental results

Target	Substrate	Substrate temperature (K)	Phases present	Reference
304L-SS	304-SS, copper	< 648	bcc	[3]
		648–773	bcc + fcc	
		> 773	fcc	
304-SS	Steel, glass	RT	bcc	[2]
316-SS			bcc	
304-SS	304-SS, rock salt	77	Amorphous	[5]
		RT	bcc + fcc	

primarily by high-resolution and analytical electron microscopy. X-ray diffractometry was used for phase identification in thick films both at room temperature and at elevated temperatures.

2. Experimental Procedure

Films of 316L stainless steel (316L-SS) were sputter-deposited on various substrates in a magnetron sputter-deposition module. Ultra-thin (4–8 nm) and thin (25–100 nm) films on thin amorphous carbon films supported by copper and beryllium grids were prepared for direct transmission electron microscopy (TEM). Thicker films (over 1 μm thick) were deposited on microscope slides for chemical analysis using energy dispersive X-ray spectrometry (EDS) and for phase determination using X-ray diffractometry (XRD). In order to study the effect of substrate nature and surface condition, films were also deposited on as-polished and oxide-free 316-SS plates.

Depositions were carried out in a constant current mode and sample-to-target distance was varied to attain deposition rates of 30–150 nm ks^{-1}. The slower rates were employed to deposit both ultra-thin and thin films, while thick films were deposited at higher rates of deposition. A few thick films were also prepared at a low rate of deposition. Generally, a 100 mA current initially required a potential of 410–430 V at the operating gas pressure of 4 Pa, but the voltage gradually dropped to about 390 V. Test samples were covered until surface contamination on the target had been sputtered off and the plasma had become stable. Depositions were performed at ambient temperature without substrate cooling. A negligible substrate heating was expected during the deposition of thin films, while a rise in the substrate temperature by as much as 20 K for thick-film deposition may have occurred [5].

3. Results

Table II gives the chemical composition for both the target and the film. There appears to be a slight enrichment of nickel and a reduction in chromium content of the film; however, the difference is only marginal. Iron, molybdenum and manganese contents are similar within the experimental scatter. No argon peak was observed in the film, implying that gas entrapment, if any, was minimal. The concentrations of nickel, chromium and iron were determined in 6 nm thick films by analytical TEM. The weight proportions of these three major constituents, 12.3:16.9:70.7, are similar within experimental error to the corresponding concentrations in the thick film, 11.8:16.5:71.6.

TABLE II Composition analysis of the film and the target

Element	Wt % in target	Wt % in film
Fe	68.5	68.4
Cr	16.4	15.8
Ni	10.6	11.3
Mo	2.2	2.5
Mn	1.9	1.7

Transmission electron microscopy of 4–8 nm thick films deposited on the amorphous carbon substrate of copper grids revealed that these films are made of extremely fine grains of the order 4–6 nm diameter. Lattice fringes were observed in some grains revealing the crystalline nature of the deposit. A selected-area diffraction pattern obtained from one such film and from an amorphous carbon substrate are shown in Fig. 1a and b, respectively. The diffraction rings coming from the deposit are thinner than the rings from amorphous carbon substrate, further showing that the deposit is crystalline. However, the *d*-spacings calculated for those lines (0.288 and 0.166 nm) did not match any known compound of iron, nickel or chromium.

Fig. 2a is a bright-field image from a 50 nm thick film showing grains having an average diameter of 6–8 nm. Analysis of a selected-area diffraction pattern, Fig. 2b, indicated that the film was comprised of a mixture of two phases: a bcc phase and an ε-martensite-like hexagonal phase. Phase identification in these films was aided by a spot pattern, shown in Fig. 3, obtained from an exceptionally large grain. All the *d*-spacings were determined after calibrating the camera constant from a diffraction pattern of a standard gold specimen. Care was taken during microscopic observation so that voltage and lens currents were kept identical for all diffraction patterns. The *d*-spacings obtained did not match any of the intermetallic compounds or solid solutions of iron, nickel, chromium, molybdenum, carbon and oxygen or various combinations of these listed in the Joint Committee on Powder Diffraction Standards (JCPDS) card files. The spot pattern clearly indicates a hexagonal (or a trigonal) symmetry. The possibility of it being an fcc diffraction pattern in the [1 1 1] beam direction was considered and subsequently eliminated, because the a_0 value obtained could not be matched to that for any known materials. Assuming that it was a diffraction pattern from a hexagonal system with the beam direction parallel to [0 0 0 1], the a_0 value calculated was twice that obtained for ε-martensite reported in literature [8]. Table III gives the *d*-spacings as determined from the ring and spot patterns and the corresponding Miller indices for bcc ferrite and Miller–Bravais indices for modified ε-phase. The lattice constant, a_0, of the modified ε-phase in the table is double the value of a_0 for ε-martensite.

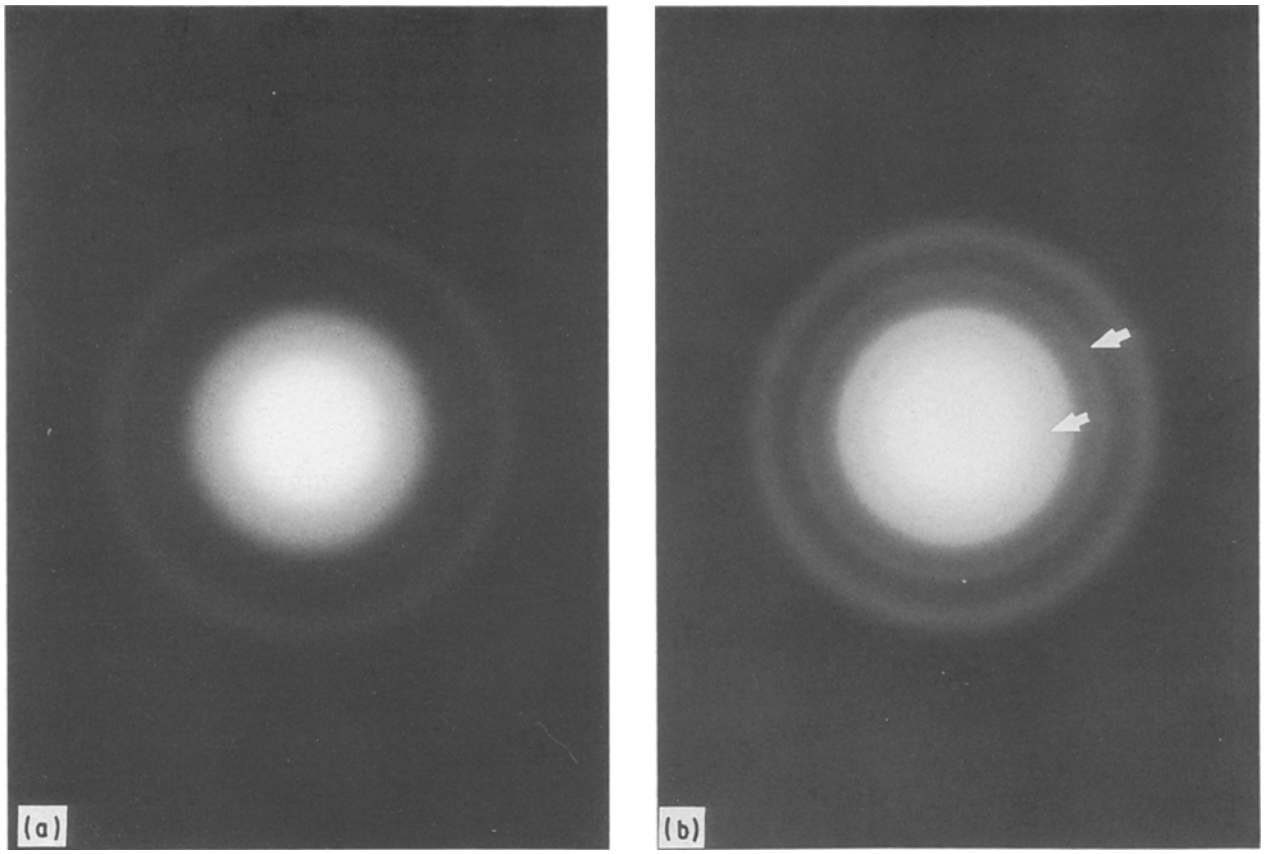

Figure 1 Selected-area diffraction patterns obtained from (a) an amorphous carbon substrate and (b) a 6 nm thick film of 316L-SS deposited on amorphous carbon. The rings from the deposit, marked by arrows, are much narrower than those from amorphous carbon.

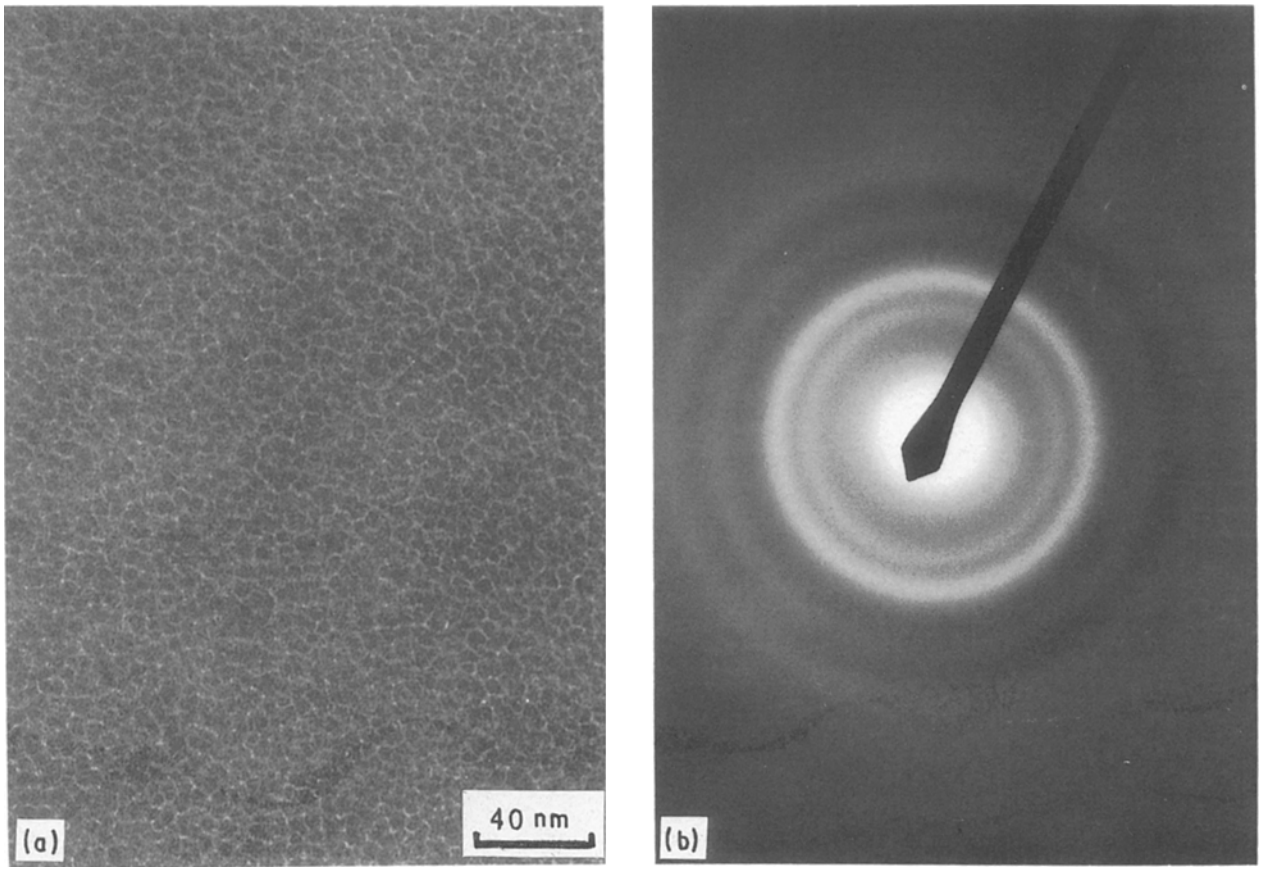

Figure 2 (a) Bright-field image of the 50 nm thick film. Average grain diameter, as seen from the image, is about 6–8 nm. (b) Selected-area diffraction pattern from the region shown in (a), indicating a randomly oriented fine-grained structure.

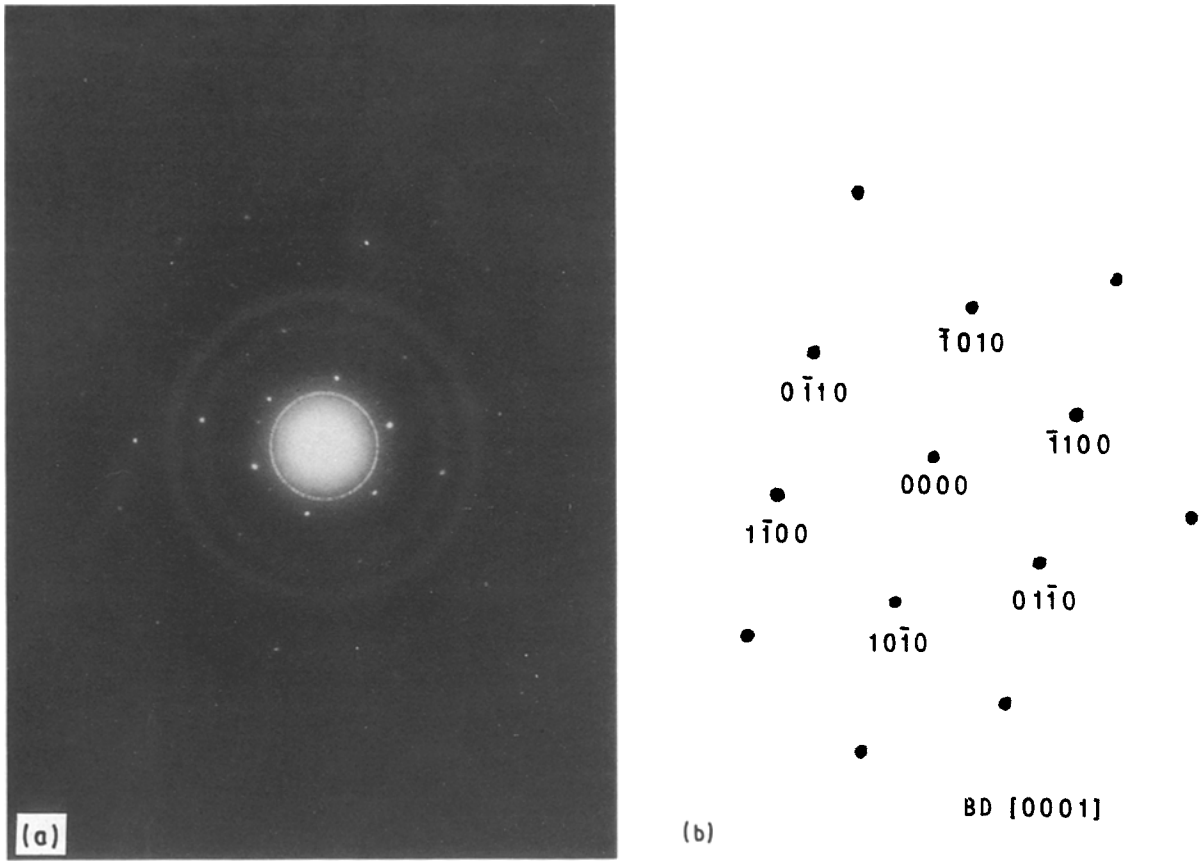

Figure 3 (a) Selected-area diffraction pattern from the large grain (spots) and surrounding fine grains (rings). (b) The beam direction for the spot pattern is [0001].

TABLE III *d*-spacings obtained form electron diffraction patterns and Miller/Miller–Bravais indices for the two phases

d-spacing (nm)	Spot/Ring	Miller indices for α-Ferrite	Miller–Bravais indices for modified ε-phase
4.438	Spot		1010
2.520	Spot + Ring		1120
2.219	Spot		2020
2.065	Ring	110	
1.634	Spot		1230
1.457	Spot + Ring	200	3030
1.260	Spot		4220
1.214	Spot + Ring		3140
0.953	Spot		4150

TABLE IV *d*-spacings obtained from X-ray diffraction pattern and Miller/Miller–Bravais indices for the two phases

2θ (deg)	*d*-spacing (nm)	Miller indices for α-ferrite	Miller–Bravais indices for modified ε-phase
35.7	2.515		1120
44.2	2.049	110	
48.8	1.866		1012
65.2	1.431	200	
75.3	1.262		2240
117.0	0.904	310	

Thicker films, approximately 1.7 μm thick, deposited on microscope slides were analysed for structure determination using X-ray diffractometry. The *d*-spacings obtained from the diffraction peaks and the corresponding Miller indices for bcc ferrite and Miller–Bravais indices for modified ε-phase are shown in Table IV. The data demonstrate that these films consist of two phases: bcc ferrite ($a_0 = 0.286$ nm) and modified hexagonal ε-phase ($a_0 = 0.504$ nm and $c_0 = 0.412$ nm). It is worth mentioning that the peak observed at $2\theta = 35.7°$ could only be explained if the a_0 value was doubled, as mentioned above.

In situ high-temperature X-ray diffraction was performed on these films. Fig. 4 shows the diffraction patterns observed at 300, 773 and 873 K. No change in

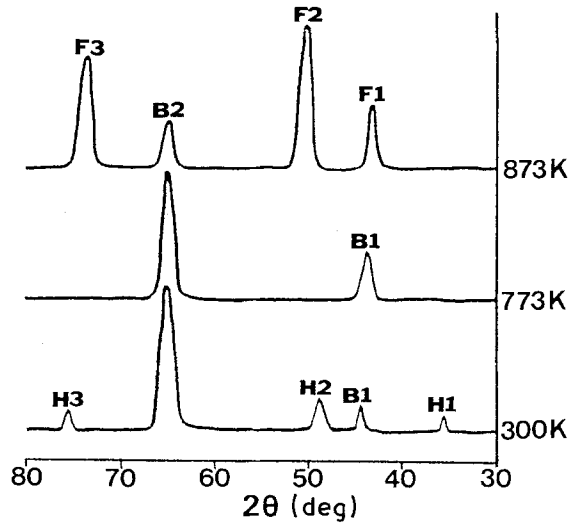

Figure 4 In situ X-ray diffraction patterns taken at 300, 773 and 873 K from a 1.7 μm thick film of 316L-SS. F1, $(1\,1\,1)_\gamma$ F2, $(2\,0\,0)_\gamma$ F3, $(2\,2\,0)_\gamma$; B1, $(1\,1\,0)_\alpha$; B2, $(2\,0\,0)_\alpha$; H1, $(1\,1.0)_\varepsilon$; H2, $(1\,0.2)_\varepsilon$; H3, $(2\,2.0)_\varepsilon$

the crystalline structure occurred upon annealing for 573 K for 18.0 ks. However, the hexagonal phase disappeared and only b c c ferrite remained when temperature was raised to 773 K. Transformation to f c c-austenite took place on annealing at 873 K. The diffraction pattern taken at room temperature revealed that the film remained austenitic after cooling.

Two 316-SS substrates were mechanically polished to a 1 μm finish. One substrate was etched with 10% HCl aqueous solution prior to inserting, within less than 30 s, in the deposition chamber. The purpose of this etching was to remove the oxide layer usually present on the surface. Another substrate was used as-polished, and simultaneous deposition was carried out under 4 Pa argon pressure and a fixed current of 100 mA to obtain a film thickness of 1.0 μm. Diffraction patterns were made in parafocusing geometry prior to and after the deposition for both substrates. Grazing angle ($\theta = 5°$) diffraction patterns were also made for both the films. The film deposited on as-polished substrate (AP-film) showed a diffraction pattern, similar to that obtained from the film deposited on a microscope slide, consisting of a mixture of b c c ferrite and modified hexagonal ε-phase. The film deposited on the etched substrate (ES-film), on the other hand, consisted mostly of b c c ferrite with a dominant ⟨2 0 0⟩ texture. The dominant texture was further confirmed by the absence of the [2 0 0] peak in the grazing angle X-ray diffraction pattern.

Microhardness measurements with 100 g load performed on AP-films yielded a diamond pyramid hardness (DPH) of 319 (± 25), whereas ES-films showed a DPH of 253 (± 15). Substrate hardness was found to be 262 (± 8). The indentations were large enough to penetrate the substrate to a depth of 3.5 μm (AP-film) and 4.0 μm (ES-film). Therefore, the hardness values obtained represent a composite hardness of film–substrate. Thus the ES-film is actually much harder than suggested by the measured value of 319. Fig. 5a and b show the indentations from AP-film and ES-film, respectively. The AP-film showed excessive cracking around the indentation, while the ES-film exhibited much less cracking. The AP-film is thus seen to be much more brittle than the ES-film.

4. Discussion

The substrate condition affects the phases that form in 316L-SS films when sputter-deposited at room temperature. The existence of a native oxide at the surface of a 316-SS substrate promotes formation of a hexagonal phase together with α-ferrite in the film. When the oxide is removed from the substrate and the substrate quickly inserted into the vacuum chamber, mostly α-ferrite forms in the sputter-deposited 316L-SS films. This helps to explain the difference between the results by Dahlgren [3] and Grundy and Marsh [5]. The *in situ* sputter-cleaning procedure used by Dahlgren most probably removed the oxide layer and therefore the b c c phase formed in the deposited film. In the work of Grundy and Marsh, the 316-SS substrate had, very likely, an oxide layer, and a two-phase

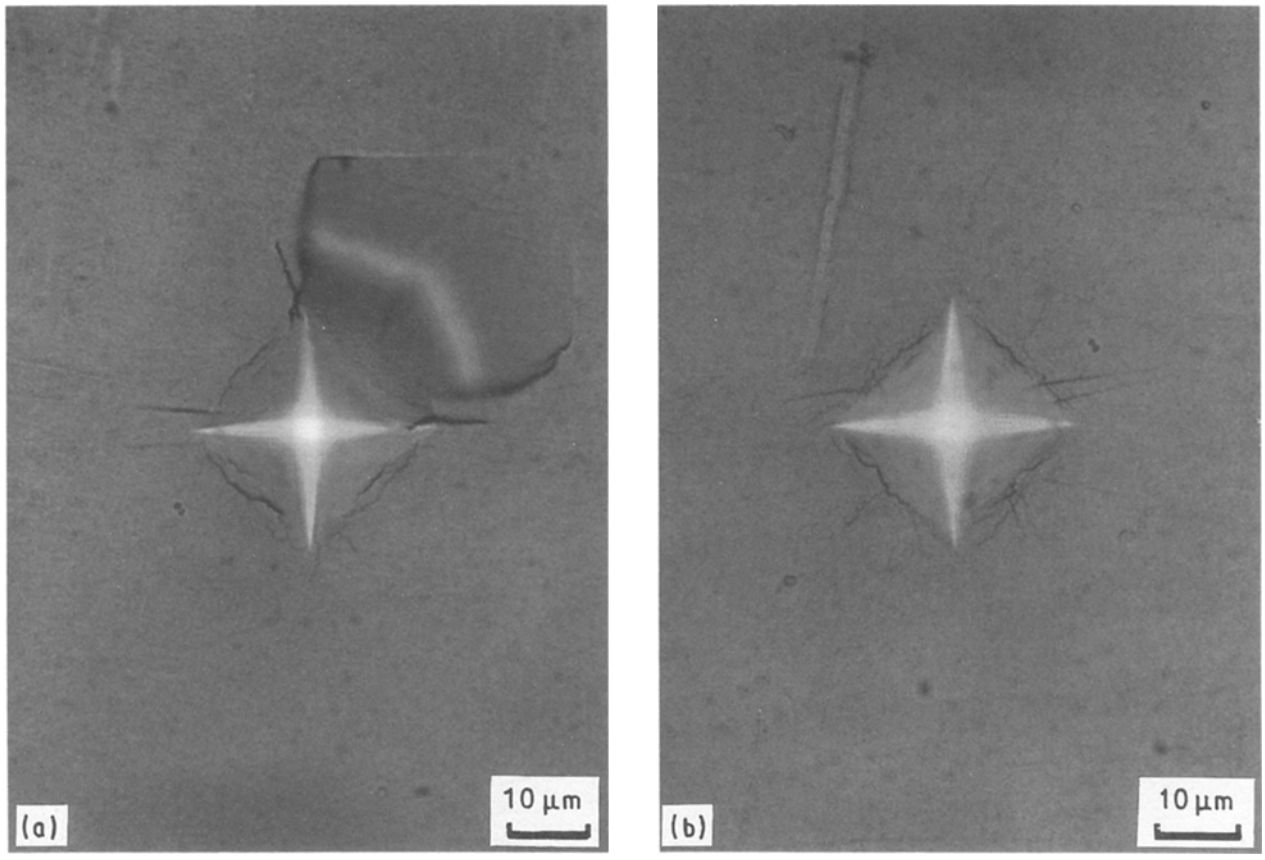

Figure 5 Vickers indentation with a 100 g load on (a) AP-film showing extensive damage around the indentation, and (b) ES-film showing much less damage around the edges of the indentation than the AP-film.

structure was obtained in the films deposited at room temperature. Glass substrates also promote formation of α-ferrite and modified hexagonal ε-phase.

The presence of a hexagonal and a b c c phase has been reported in earlier studies where different grades of stainless steels were either quenched or subjected to plastic deformation [9–12]. The hexagonal phase observed in this study bears close resemblance to the hexagonal ε-phase, except that in order to explain all the electron diffraction spots and rings and X-ray diffraction peaks, the a_0 lattice constant had to be twice that of ε-martensite. This double lattice constant suggests that ordering took place in the hexagonal phase during film deposition. Because the proportion of iron atoms to the other alloying elements nearly 2:1, it is possible that the nickel and chromium atoms occupy every third row in the basal plane, giving rise to the unique ordering. The composition of the hexagonal phase could not be determined because the grains are extremely small and no individual grains that could be identified as having a hexagonal structure are discernible.

It is difficult to invoke kinetic reasons in a deposition process to explain the formation of one crystalline phase over the other if the two phases have the same chemical composition. This is particularly true in the case of the formation of the α-phase on an austenitic substrate. Nucleation could have been avoided if an austenitic film had grown epitaxially on an austenitic substrate. The reason why a ferritic film grew on austenitic 316-SS must therefore be related to phase stability. This argument is consistent with the formation of a b c c phase (martensite) by plastic deformation of 316L-SS at low temperatures. The mobility in the solid state is so low that both nucleation and growth are inhibited and a special type of mechanism (martensitic transformation) is required for the f c c to b c c transformation to take place.

The annealing experiments show that the α-phase is stable at temperatures below 873 K, while the two-phase field (α- and hexagonal ε-phase) has an upper limit of 773 K. Kelly *et al.* [13] calculated the Gibb's free energy difference between austenite and ferrite in austenitic 303-SS. The b c c phase was found to be stable up to 840 K and then again at higher temperatures. The temperature of 840 K is fairly close to the temperature where transformation from b c c to f c c was observed in our 316L-SS films. The 303-SS contains approximately 2% less nickel and 1.6% less molybdenum.

Frank's model of the martensitic transformation shows that a good matching of the b c c (1 1 0) and f c c (1 1 1) planes can be obtained if they meet in a given plane which is the habit plane for the transformation. Although no transformation is occurring here, this model suggests that b c c phase could grow epitaxially without the need to go through a nucleation stage. If the substrate surface presents an amorphous or an oxide layer, then nucleation should be necessary, and in that case another competing phase, e.g. the observed hexagonal ε-phase, can also nucleate and grow. This leaves two possibilities for the formation of the b c c phase. One is that it nucleates on its own, the other is that the hexagonal phase may assist the b c c nucleation. For instance, there is evidence that there is a sequence of martensitic transformation in austenitic stainless steels from $\gamma \rightarrow \varepsilon \rightarrow \alpha$ [14]. The strong texture observed in the film is probably due to preferential growth and corresponds to the dendritic growth direction in the solidification of b c c metals [15].

Acknowledgements

This project was sponsored in part by the Electrical Power Research Institute Grant no. RP8011-02, by the National Science Foundation Grant no. DMR-8900417 and in part by the US Department of Energy, Assistant Secretary for Conservation and Renewable Energy, Office of Transportation Technologies, as part of the High Temperature Materials Laboratory User Program, under contract DE-AC05-840R21400 managed by Martin Marietta Energy Systems, Inc.

References

1. T. ANGEL, *J. Iron Steel Inst.* **177** (1954) 165.
2. S. MALAVASI, A. OUELDENNAOUA, M. FOOS and C. FRANTZ, *J. Vac. Sci. Technol. A* **5** (1987) 1888.
3. S. D. DAHLGREN, *Met. Trans.* **1** (1970) 3095.
4. R. WANG, *J. Mater. Sci.* **17** (1982) 1142.
5. P. J. GRUNDY and J. M. MARSH, *ibid.* **13** (1978) 677.
6. J. CHILDRESS, S. H. LIOU and C. L. CHIEN, *J. Appl. Phys.* **64** (1988) 6059.
7. S. CRAIG and G. L. HARDING, *J. Vac. Sci. Technol.* **21** (1982) 1142.
8. J. F. BREEDIS and W. D. ROBERTSON, *Acta Metall.* **10** (1962) 1077.
9. W. O. BINDER, *Metal Progr.* **58** (1950) 201.
10. B. CINA, *J. Iron Steel Inst.* **177** (1954) 406.
11. B. CINA, *Acta Metall.* **6** (1958) 748.
12. H. M. OTTE, *ibid.* **5** (1957) 614.
13. T. F. KELLY, M. COHEN and J. B. VANDER SANDE, *Met. Trans.* **15A** (1984) 819.
14. P. L. MANGONON Jr and G. THOMAS, *ibid.* **1** (1970) 1587.
15. B. CHALMERS, *Trans. AIME* **200** (1954) 519.

Received 11 July 1991
and accepted 17 February 1992